ELECTRICALLY ADDRESSABLE VESICLES – TOOLS FOR DIELECTROPHORESIS METROLOGY

Salil P. Desai, **Michael D. Vahey**, and **Joel Voldman**[*]
Department of Electrical Engineering and Computer Science Massachusetts Institute of Technology, Cambridge, MA 02139

Abstract

Dielectrophoresis (DEP) has emerged as an important tool for the manipulation of bioparticles ranging from the submicron to the tens of microns in size. Here we show the use of phospholipid vesicle electroformation techniques to develop a new class of test particles with specifically engineered electrical properties to enable identifiable dielectrophoretic responses in microfabricated systems. These electrically addressable vesicles (EAVs) enable the creation of electrically distinct populations of test particles for DEP. EAVs offer control of both their inner aqueous core and outer membrane properties; by encapsulating solutions of different electrolyte strength inside the vesicle and by incorporating functionalized phospholipids containing PEG brushes attached to their hydrophilic head group in the vesicle membrane, we demonstrate control of the vesicles' electrical polarizabilities. This combined with the ability to encode information about the properties of the vesicle in its fluorescence signature, form the first steps toward the development of EAV populations as metrology tools for any DEP-based microsystem.

INTRODUCTION

Giant unilamellar vesicles (GUVs) have garnered considerable interest as both model cellular compartments and model membranes. GUVs have been used as model systems for studying a range of cellular phenomena and machinery ranging from cellular compartmentalization[1,2], actin polymerization[3], gene expression[4] and membrane fusion[5]. GUVs serve as good model systems due to their large size (1 − 100 μm) and ease of visualization with conventional light microscopy. They also offer exquisite control over both their inner aqueous core and outer membrane properties. Various techniques have been explored for encapsulating particles and molecules ranging from mammalian cells[6] to large DNA strands[7] within the aqueous core of vesicles. Additionally, standard formation techniques for GUVs allow for the creation of complex mixtures of lipids and small molecules within the membrane[8,9]. We have leveraged this inherent flexibility in the preparation of GUVs to generate vesicles with distinct electrical properties which have identifiable dielectrophoretic responses. By modulating these electrical properties we have demonstrated the concept of electrically distinct vesicle populations to serve as test particles for dielectrophoresis (DEP) based microsystems. We term these new test particles as electrically addressable vesicles (EAVs).

[*] To whom correspondence should be addressed: (617) 253−2094 (Phone) / (617) 258−5846 (Fax) / voldman@mit.edu (email).

SUPPORTING INFORMATION AVAILABLE:
To further elucidate key points from this work we include a plot showing the EAV core conductivity sensitivity as a function of changes in EAV radius and image processing of PEGylated EAVs to confirm uniform PEG-lipid incorporation in EAVs. This material is available free of charge via the Internet at http://pubs.acs.org.

Although much recent work on GUVs has focused on the dynamics and structure of the vesicles themselves, the potential of engineering the electrical properties of vesicles has been largely unexplored. The ability to control the composition of the aqueous core and membrane, in addition to enabling the study of membrane biophysics, also allows for the creation of vesicles spanning a wide range of electrical and mechanical properties. Accordingly, any system intended to manipulate cells or particles on the basis of their electromechanical properties can be characterized more thoroughly by using test particles specifically designed to encompass the entire range of these properties.

DEP-based microsystems are widely used for patterning[10-12], concentrating[13-15] or sorting[16-18] cells. DEP - the force on a polarizable object in a spatially nonuniform electric field - depends on the electric field and the electrical properties of the particle (assumed to be spherical) relative to the surrounding medium. The dipole contribution to the DEP force is given by the equation

$$\mathbf{F}_{\text{DEP}} = 4\pi\varepsilon_m a^3 \quad \text{Re}\left\{\underline{K}(\omega)\right\} \mathbf{E} \cdot \nabla\mathbf{E}$$

(1)

Here, ε_m denotes the permittivity of the medium, a denotes the particle radius, $\mathbf{E}$ denotes the electric field, and $\underline{K}(\omega) = \left(\underline{\sigma}_p - \underline{\sigma}_m\right) / \left(\underline{\sigma}_p + 2\underline{\sigma}_m\right)$ is the Clausius-Mossotti function, a dimensionless factor describing the frequency-dependent electrical properties of the particle $\left(\underline{\sigma}_p = \sigma_p + i\omega\varepsilon_p\right)$ and medium $\left(\underline{\sigma}_m = \sigma_m + i\omega\varepsilon_m\right)$. Since the induced dipole moment of a particle is proportional to Re$\{\underline{K}\}$, knowing the Clausius-Mossotti function for a specific set of particles is critical to determining the magnitude and sign of the DEP forces throughout a system. A prerequisite for knowing the Clausius-Mossotti function is to know the particles' structure, electrical conductivity, and electrical permittivity.

Current test particles for DEP consist primarily of polystyrene microspheres, which are commercially available in several sizes and with various surface functionalizations (for example, carboxyl groups). While functionalized microspheres (FMs) can be further engineered with phospholipids in an effort to mimic biological membranes[19] they poorly mimic the electrical properties of live cells. This is largely attributable to the disparity between the bulk conductivity and permittivity of polystyrene and that of a cell's cytoplasm; polystyrene lends the particles a negative polarizability at high frequencies (~1 MHz) in nearly any aqueous solution. Furthermore, because the electrical properties of FMs are controlled primarily through the charge density presented at the surface of the particle, tailoring beads to exhibit a specific conductivity is generally not straightforward and may require potentially laborious sequences of reactions to achieve the desired electrical response. To circumvent some of these difficulties, it is possible to take the notion of surface modification to its extreme by coating otherwise electrically insulating particles with a conductive metal layer. These metal-coated particles then present an alternative to the low conductivity and permittivity of polystyrene relative to water. Although such particles have been successfully employed in testing systems where positive dielectrophoresis (pDEP) is essential[16], they are not as widely used as FMs. This may be attributable to the fact that they exhibit nearly uniform positive polarizability regardless of the frequency of the applied field or the conductivity of the surrounding medium. In addition to FMs, multi-layered lipid-based particles such as multilamellar and oligolamellar vesicles have been used in electrorotation experiments to verify dielectric multi-shelled models for cells[20]. While such multi-shelled particles can serve as surrogates for cells (particularly bacterial and yeast cells which possess a multi-layered cell wall), they can be challenging to

reliably replicate and are therefore not well-suited for building electrically-distinct populations as test particles for DEP-based systems.

For many applications, a particle whose dielectrophoretic response is sensitive to its environment - both electric field frequency and medium electrical properties – is desirable. EAVs offer an alternative in which both the bulk properties of the particle (i.e. the aqueous core) as well as its membrane may be tailored to exhibit a particular DEP spectrum. EAVs enable the generation of test particles over a large range of conductivities (varying over ~100× of physiologically relevant conductivities) which cannot be achieved easily with commercially available FMs. The additional ability to label EAVs with membrane-bound or internalized aqueous fluorescent markers allows information regarding the vesicle's properties to be encoded so that vesicles can be visually identified. Taken together, the degrees of freedom afforded by EAVs with respect to their electrical polarizability and fluorescent signatures make these particles compelling model systems for characterizing DEP-based microsystems.

RESULTS

Creating EAVs

We have generated EAVs with customizable electrical properties through the process of electroformation[21]. Figure 1A shows a schematic of EAVs in which the composition of both the aqueous core and phospholipid membrane may be tuned independently (or in concert) to confer distinct electrical properties to a vesicle population. The electrical properties of the aqueous core are readily tuned in the electroformation process, by controlling the conductivity of the electroformation buffer and thereby conferring a specific internal conductivity, σ_c, to the formed vesicles. Therefore, by leveraging the electroformation process, it is straightforward to vary the value of σ_c over a broad range. Specifically, we have successfully formed vesicles in solutions ranging in conductivity from ~10^{-4} S/m (deionized water) to ~1.5 S/m (1× phosphate buffered saline, ionic strength ~150 mM), though we have observed that the size and yield of electroformed vesicles diminishes at higher conductivities (typically above ~0.1 S/m). Without significantly altering the conductivity or size distribution, we have also encapsulated fluorescent dyes, including fluorescein (Figure 1B, inset) and rhodamine. The encapsulation of fluorescent dyes facilitates the tagging of vesicles of specific conductivity with an identifiable fluorescence spectrum.

An additional degree of freedom in creating vesicles with distinct dielectric spectra is conferred by the phospholipid membrane. Long chain polymers (such as PEG) can be conjugated to the membrane bilayer to change its dielectric properties. PEG brushes serve to modulate the effective membrane thickness and consequently the membrane capacitance conferring unique electrical properties to a vesicle population. Like the aqueous core, the vesicle membrane is also capable of supporting fluorescent labels. Figure 1B depicts a representative vesicle formed with a fluorescently-labeled phospholipid, and Figure 1C shows a merged fluorescence image of sample EAV populations and indicates the ability to optically distinguish between differentially labeled EAVs. The ability to label vesicles not only allows us to encode information about the properties of the EAVs in their fluorescence signature, but facilitates the tracking and visualization of EAVs in microsystems.

Biasing EAV size

As is evident from Figure 1B, electroformation techniques yield EAVs with a wide range of sizes. To narrow the size distribution of EAVs and tailor them to the DEP system being characterized, we performed filtrations using syringe-attached inline glass frit filters (of 5 μm and 10 m pore sizes). Figure 2A shows quantitative results for sizes of EAVs filtered through 5 and 10 μm pores (where sizes were measured using light microscopy). Filtration through a

5 μm pore allows for narrowing the mean EAV size from 4.6 μm to 1.8 μm whereas filtration through a 10 μm pores tunes the EAV size from 4.6 μm to 3.4 μm. The fluorescence images in Figure 2B show qualitative agreement with these results. The top panel shows unfiltered EAVs (labeled with lissamine rhodamine for fluorescence visualization) and the middle panel shows a fluorescence image after filtration through a 5 μm pore where few large (>10 μm) vesicles are visible indicating that they were blocked or ruptured in the glass frit filter. The bottom panel shows a representative fluorescence image after filtration through a 10 μm pore where several large vesicles are still visible. These results indicate that filtration can bias the EAV size distribution and thereby create vesicle populations that are amenable for use in microsystems. In the following sections we describe the ability to use polydisperse EAV populations for use as test particles for DEP

EAVs as test particles

The structure of electroformed GUVs, comprised of an internal aqueous core surrounded by a lipid bilayer membrane, lends these particles a dielectric spectrum which is qualitatively (and potentially quantitatively) similar to that of live cells. This spectrum is characterized by both high- and low- frequency dispersions, and in the case of EAVs, may be controlled through the conductivity of the aqueous core, σ_c. By varying σ_c, it is possible to create test particles with specifically engineered spectra; this is in contrast to many widely available alternative test particles, including both metallic and polystyrene beads, which tend to have uniformly negative and positive dielectrophoretic spectra, respectively. Accordingly, it is possible to create EAVs for which the transition from negative to positive polarizability occurs at a controlled frequency (Figure 3A).

In addition to offering spectra distinct from commercially available microspheres, EAVs offer the ability to create suspensions of particles that are both visually and electrically distinct by varying the membrane-bound fluorophore and the conductivity of the internal solution. Figure 3A shows an experiment in which EAVs labeled with rhodamine (red) and carboxyfluorescein (green) and encapsulating different conductivities (0.1 and 80 mS/m, respectively, with a medium conductivity of 40 mS/m) respond differently to the application of an electric field at a frequency of 1 MHz. In this part of the spectrum, vesicles with internal conductivities in excess of the medium conductivity ($\sigma_c > \sigma_m$) exhibit positive polarizability and are attracted to the electrode edge, whereas vesicles with less conductive cores are negatively polarizable and are repelled to the regions above and between the electrodes. Figure 3B presents a related demonstration, where we used red fluorescent polystyrene microspheres to demonstrate the more complex electrical properties that EAVs can present. While the microspheres exhibit a flat dielectric spectrum over a broad range of frequencies, the EAVs undergo a dispersion at ~200 kHz, going from negative polarizability at 50 kHz to positive polarizability at 500 kHz. Figure 3C illustrates in greater detail the dielectrophoretic spectrum of an EAV suspension comprising a range of sizes. At 50 kHz, these vesicles have a strong negative polarizability, which weakens as the frequency is increased to 100 kHz. By 500 kHz, nearly all vesicles exhibit positive polarizability, a condition that persists up to about 2 MHz, where the higher of the two crossover frequencies is observed. These dielectrophoretic spectra demonstrate the ability of EAVs to encompass a more complex set of electrical properties than other commonly used test particles for DEP.

Determining membrane characteristics from cross-over frequency

To characterize the electrical properties of individual EAVs and to compare these properties to those predicted by established theories for single-shelled spherical particles[22], we perform a series of crossover frequency measurements. This allows us to determine the conditions under which the EAVs' polarizabilities vanish[23]. Because we have experimental control over the conductivity and permittivity (σ_c and ε_c respectively) of the EAV core, we focus on the

properties of the membrane, which we assume is described by a permittivity ε_{mem} and thickness δ. In a medium of conductivity σ_m and permittivity ε_m, the complex Clausius-Mossotti function at frequency ω for a vesicle is given by:

$$\underline{K}(\omega) = \frac{-\sigma_m\sigma_c + iw\left[ac_m(\sigma_c - \sigma_m) - (\sigma_c\varepsilon_m + \sigma_m\varepsilon_c)\right] - \omega^2\left[ac_m(\varepsilon_c - \varepsilon_m) - \varepsilon_c\varepsilon_m\right]}{2\sigma_m\sigma_c + i\omega\left[ac_m(\sigma_c + 2\sigma_m) + 2(\sigma_c\varepsilon_m + \sigma_m\varepsilon_c)\right] - \omega^2\left[ac_m(\varepsilon_c + 2\varepsilon_m) + 2\varepsilon_c\varepsilon_m\right]} \tag{2}$$

where a represents the radius of the vesicle and $i = \sqrt{-1}$. The form of Eq. 2 comes from the standard formulation for a sphere bounded by a thin membrane[22]. Here, we have combined the membrane properties into a single capacitance-per-unit-area ($c_m \equiv \varepsilon_{mem}/\delta$). We neglect the effects of membrane conductance (g_m) on the assumption that it has little effect on the membrane's electrical properties at frequencies down to a few kilohertz (typical values of g_m are on the order of ~1 S/m^2 with $c_m \sim$ 0.02 F/m^2). Additionally, we have neglected any contribution arising from the vesicles' surface conductance; for a vesicle with a surface conductivity of ~0.1 nS (typical for a charged bilayer membrane) and a radius of ~1 μm, the surface conductance will contribute ~0.2 mS/m to the particle's overall conductivity – roughly ~1% of the typical conductivities used in our experiments. To simplify Eq. 2, we begin by addressing only the low-frequency behavior of the polarizability. This allows us to focus more directly on the contribution of the membrane to the vesicles' dielectrophoretic response. In this frequency regime, Eq. 2 simplifies to:

$$\underline{K}(\omega) = \frac{-\sigma_m\sigma_c + i\omega\left[ac_m(\sigma_c - \sigma_m) - (\sigma_c\varepsilon_m + \sigma_m\varepsilon_c)\right]}{2\sigma_m\sigma_c + i\omega\left[ac_m(\sigma_c + 2\sigma_m) + 2(\sigma_c\varepsilon_m + \sigma_m\varepsilon_c)\right]} \tag{3}$$

This expression is valid provided the frequency is significantly lower (i.e. by about one decade) than the inverse of the charge relaxation times for both the vesicle interior and exterior ($\omega \ll \sigma_c/\varepsilon_c$ and $\omega \ll \sigma_m/\varepsilon_m$, respectively). Using (3) and setting $\text{Re}\{\underline{K}(\omega_0)\} = 0$, we find an expression for ω_0, the lower of the two possible cross-over frequencies permitted by Eq. 2:

$$\omega_0^2 = \frac{2(\sigma_m\sigma_c)^2}{\left[ac_m(\sigma_c - \sigma_m) - (\sigma_c\varepsilon_m + \sigma_m\varepsilon_c)\right]\left[ac_m(\sigma_c + 2\sigma_m) + 2(\sigma_c\varepsilon_m + \sigma_m\varepsilon_c)\right]} \tag{4}$$

To better understand the properties of the EAV membrane, it is convenient to rearrange Eq. 4 so as to relate the crossover frequency, which we observe directly, to δ, the membrane thickness:

$$\delta = 2a\varepsilon_{mem}\frac{(\sigma_c - \sigma_m)(\sigma_c + 2\sigma_m)}{\sigma_c(\sigma_c\varepsilon_m + \sigma_m\varepsilon_c)}\left[4\frac{\sigma_m}{\sigma_c} - 1 + 3\left[1 + \frac{8\sigma_m^2(\sigma_c - \sigma_m)(\sigma_c + 2\sigma_m)}{9\omega_0^2(\sigma_c\varepsilon_m + \sigma_m\varepsilon_c)^2}\right]^{1/2}\right]^{-1} \tag{5}$$

Measuring crossover frequency across different core and medium conductivities (σ_c and σ_m), and across different batches of electroformed EAVs yields an effective membrane thickness of 9.3 ± 4.3 nm. The sensitivity of δ to ω_0 for typical parameters is such that a 10% change in crossover frequency produces a change of ~8% in predicted membrane thickness. Our measurements are in reasonable agreement with expectation for the thickness of a lipid bilayer and support the validity of this simple model for vesicle polarizability. Specifically, we find that extracted values of δ are fairly independent of the vesicle radius (correlation coefficient: −0.0026 across 80 individual vesicles) as well as the crossover frequency (correlation coefficient: 0.18). While low coefficients of correlation are not sufficient to prove

independence, they do suggest that our measurements are consistent with the functional dependencies of δ on these parameters given by Eq 5. Additionally, we find that the specific fluorophore incorporated in the membrane does not lead to a change in electrical properties, with carboxyfluorescein-labeled and rhodamine-labeled vesicles exhibiting no observable difference in crossover frequency (not shown).

Modulating membrane capacitance

In addition to the ability to control the electrical properties of the EAVs through their aqueous core, we also demonstrate the ability to modify the vesicles' dielectric spectra through the structure and composition of their membrane (Figure 4A). Since the thickness and dielectric constant of the lipid membrane is fairly constant over a wide range of lipids, we decided to alter the membrane properties by incorporating into the membrane lipids conjugated with polymers, which would increase the effective membrane thickness while also altering its effective dielectric constant. We incorporated 5 mole-percent PEG-modified fluorescently tagged lipid into our membranes to verify this hypothesis. The presence of a fluorescence signal in the membrane (Figure 4A, inset) indicates that the PEG-modified lipid indeed organizes in to the membrane of the vesicle. Additionally, we counter-stained PEGylated EAVs with lissamine-rhodamine labeled fluorescence to confirm that the incorporation of PEG is comparable across vesicles of different sizes. Specifically, we used image processing techniques to quantify the average fluorescence in the membrane for vesicles ranging in size over an order of magnitude. We found that the average fluorescence intensity over this size range is within 5% indicating that the PEG-lipid concentration across vesicles is uniform (data not shown). As shown in Figure 4B, these membrane-modified EAVs displayed different electrical properties than unmodified EAVs. Using the same method for measuring the sizes and crossover frequencies of individual EAVs and interpreting the results in the context of a single-shell spherical model (Eq. 5), we are able to discern changes in the low-frequency dielectrophoretic response of the EAVs. While the unmodified EAVs exhibit crossover frequencies consistent with the previously discussed single shell model, PEG-functionalized EAVs deviate from this pattern suggesting that a more complex model is needed to accurately describe their electrical properties, such as a multi-shell model[20] incorporating separate lipid and PEG layers. As mentioned previously, when fit to the single shell model, we extract a membrane thickness for the unmodified vesicles that is independent of particle radius and consistent in value (~5−10 nm) with expectations for a phospholipid bilayer. In contrast, extracted membrane thicknesses for PEG-functionalized vesicles increase with vesicle radius. We are able to reliably detect the increase in crossover frequency of PEG-functionalized EAVs over their non-functionalized counterparts associated with this change; however, the increasing extracted membrane thickness suggests that the single shell model of Eq. 5 with the membrane thickness δ independent of all other parameters is no longer sufficient to describe the membrane capacitance of PEG-functionalized EAVs. This may be attributable to differences in PEG conformations within membranes of different curvature, or to the effects of PEG on membrane morphology. Additionally, we electroformed PEG-functionalized EAVs with low concentrations (0.1 mole-percent) of PEG. Cross-over frequency measurements were made with these EAVs and the results were compared to those predicted from a single-shell model. Effective membrane thicknesses extracted from these comparisons yielded 8.4±2.3 nm, which is of the same order as EAVs without incorporation of PEG. This suggests that a mole percentage of at least a few percent PEG may be necessary to obtain particles with a well-organized PEG-brush and consequently a significantly altered membrane capacitance.

To determine the predicted PEG-functionalized EAV membrane thickness we considered the physicochemical properties of PEG polymers that would govern their morphology and organization within the lipid bilayer membrane. The physicochemical aspects of lipid membranes with grafted polymers have been the subject of considerable past study[24]. Based

on the concentrations and molecular weight of PEG-lipid used in our experiments, we expect that the PEG organization structure is above the "mushroom-to-brush" structural transition point. Hence, in our case the PEG lipids assume a stretched, brush-like configuration in which the PEG chains extend out from the membrane surface. As previously determined[24], the transition between the mushroom and brush regimes occurs at the concentration of PEG-lipid for which the surface-associated polymer chains first begin to overlap. This condition is fulfilled at mole fractions of polymer lipid given by, $X_{PEG}^{m \to b} > \left(A_1/\pi a_m^2\right) n_p^{-6/5}$, where, A_1 is the membrane surface area per lipid molecule, a_m is the size of the monomer unit and n_p is the degree of polymerization. Based on these parameters (which are extensively explored by Marsh, *et al.*[24]) the mushroom to brush transitions for PEG lipids for molecular weight of 2000 (as in our case) occurs at mole percentages of 0.5% above (the mushroom configuration is typically only relevant for low molecular weight lipids with short chain lengths). Further the anticipated membrane thickness can be derived from the minimization of the free energy of the membrane[25], and is determined as previously described[24] by, $L \approx n_p a_m^{5/3} (X_{PEG}/A_1)^{1/3}$. This effective PEG brush thickness (*L*) is determined from the above equation as 5.02 nm, using $n_p = 45$ (from Marsh, *et al.*[24]), $a_m = 0.39$ nm (determined from the monomer volume in aqueous solution[26]), $X_{PEG} = 0.1$ (from Marsh, *et al.*[24]), $A_1 = 0.65$ nm^2 (from Marsh[27]). This is in good agreement with X-ray diffraction measurements of the thickness of comparable PEGylated di-stearoyl-phosphatidylcholine (DSPC) lipid bilayer measurements[28] which report a thickness of 5.6 nm. As the PEG brush extends outward from both the inner and outer leaflets of the membrane it is incorporated twice (~ 10 nm total brush thickness) along with the estimation of the effective membrane thickness of an unmodified EAV (as ~ 5 nm) yielding ~ 15 nm total estimated membrane thickness. Further, this anticipated membrane thickness fits well with our measurements of effective membrane thickness of PEGylated EAVs of ~ 20 nm (for smaller vesicle sizes, as seen in Figure 4B). The discrepancies of larger effective membrane thickness for larger PEGylated EAVs (as seen in Figure 4B) could arise from steric interactions of PEG polymers in the brush regime. Such interactions have been known to exert lateral pressures to expand the lipid membrane[24] and have been experimentally verified[29].

DISCUSSION

Our results demonstrate the feasibility of creating populations of particles with distinct and controllable optical and electrical properties. These results should open new avenues in both the characterization of dielectrophoretic traps and in the electrical manipulation of vesicles. Previously, DEP traps have been primarily characterized with polystyrene microspheres, which prove to be constraining in their electrical properties. Additional functionalizations and surface chemistry[19] have been performed but they can involve considerable complexity, which makes the route to multiplexing more difficult. Conductive test particles such as metal or metal-coated microspheres are challenging to fabricate and are commercially available in a very limited size range. Thus, most systems that leverage these highly conductive particles use pDEP and are limited to nanometer-scale particles, (e.g. for self-assembly[30]). Hence, EAVs fill a much needed void in the application space in metrology tools for characterizing DEP traps.

We have shown that EAVs have unique advantages over conventional test particles. However, they do have some limitations that impact the design of electrically distinct populations, specifically, the size polydispersity that results from electroformation. Nonetheless, electroformation has been the predominant technique for the generation of vesicles even though several alternate techniques for formation of vesicles have emerged. These techniques range from lipid film patterning[31], to pulsatile jet flow[32] and microfluidic sheathing flows[6]. To the best of our knowledge, none of these techniques is capable of generating giant vesicles in the typical size range of cells, 10 − 25 μm. For example, the pulsatile jet flow techniques typically produce vesicles of very large size (> 100 μm), which would preclude their use in DEP-based

microsystems for manipulating cell-sized bioparticles in the 1−50 μm size range. The generation of monodisperse vesicles in the size range of typical cells continues to be a major research challenge. To circumvent this challenge we describe techniques for the use of EAVs that are applicable even in the case of polydisperse vesicle populations.

Since electroformation is the predominant method of vesicle formation, it is important to understand how to design desired electrical properties in vesicle populations in the presence of size polydispersity. Size impacts electrical properties by affecting the membrane capacitance of the resulting particle; specifically, larger vesicles exhibit larger membrane capacitances and thus their low frequency dispersion occurs at lower frequencies than that of smaller vesicles. Eq. 3 shows that the crossover frequency may vary strongly with variations in the vesicle radius, a, with $\omega \propto a^{-1}$ for larger vesicles (typically corresponding to $a \sim 1-10$ μm). Thus, to design a population with a known dielectric response, one approach is to operate at the plateaus of the dielectric spectra rather than near the crossover frequency, since the plateaus are less affected by size (Figure 3C).

Alternatively, operating at high frequency allows the electrical properties of the vesicle to be dominated by the vesicle's internal conductivity and permittivity, which are very well controlled. For intermediate- to high frequencies, the crossover frequency is determined approximately from:

$$\omega_0^2 = \frac{[ac_m(\sigma_c - \sigma_m) - (\sigma_c\varepsilon_m + \sigma_m\varepsilon_c)][ac_m(\sigma_c + 2\sigma_m) + 2(\sigma_c\varepsilon_m + \sigma_m\varepsilon_c)]}{[ac_m(\varepsilon_m - \varepsilon_c) + \varepsilon_c\varepsilon_m][ac_m(\varepsilon_c + 2\varepsilon_m) + 2\varepsilon_c\varepsilon_m]}$$

(6)

For sufficiently large vesicles (for which $ac_m \gg \varepsilon_m, \varepsilon_c$), equation (6) becomes independent of the vesicle size, reducing to $\omega_0^2 = (\sigma_c - \sigma_m)(\sigma_c + 2\sigma_m)(\varepsilon_m - \varepsilon_c)^{-1}(\varepsilon_c + 2\varepsilon_m)^{-1}$.

The creation of two distinct EAV populations is most easily achieved by selecting the internal conductivity of one vesicle to be below that of the surrounding medium so that its polarizability is uniformly negative at all frequencies, while the other vesicle population, with internal conductivity higher than the surrounding medium, will exhibit polarization that will be positive over some (programmable) frequency range. The difference in the internal conductivity of the vesicle and that of its surrounding solution can result in an osmotic gradient. A vesicle is in osmotic equilibrium when the osmotic pressure drop arising from the solute concentration difference is balanced by the Laplace pressure arising from the tension of the membrane. This leads to the equilibrium condition $RT(c_i - c_o) = -2\gamma/a$, where R is the ideal gas constant, T is the absolute temperature, c_i and c_o are the internal and external osmolarities (respectively), γ is the membrane tension, and a is the vesicle radius. In our experiments, the difference in osmolarity is on the order of 0.5 mM (1× PBS diluted by a factor of $\sim$300×), with the higher osmolarity typically inside the vesicle, driving the flux of water into the vesicle and causing it to swell. For the membrane tension, we assume that the membrane tension $\gamma = \kappa\backslash(A/A)$, is the product of the elastic area expansion modulus (κ) and the fractional change in membrane area. For a 20 μm diameter vesicle with $\kappa \sim 360$ dynes/cm[33], the fractional change in area is under 3.5%, corresponding to a fractional change in volume of $\sim$5%. Although a 5% increase in vesicle volume would create a corresponding decrease in the internal conductivity, in cases where the internal and external conductivities differ by $\sim$2× this does not significantly influence the vesicles' dielectrophoretic response. Accordingly, in interpreting our experiments, we have neglected this effect. Since vesicles typically cannot withstand fractional area changes of $\sim$10% (a volume change of $\sim$15%), vesicles will typically rupture before the flux of water entering the vesicle has a substantial effect on the internal conductivity. Furthermore, osmotic stress can be mitigated altogether through the addition of non-ionic solutes (e.g. sucrose or glucose) to the internal or external phases.

Besides limitations on the osmolarity difference between internal and external solutions that the vesicle membrane is able to support are considerations regarding the electrical permittivity of the internal and external solutions that can be used. Specifically, the use of solvents significantly less polar than water can fundamentally interfere with the stability of the vesicle membrane. Accordingly, the degree of control one may exercise over the core and medium permittivities of the EAVs, ε_c, and ε_m, respectively is much more limited than that possible for their corresponding electrical conductivities.

In the case where more than two vesicle populations with distinct spectra are desired, the choice of the internal conductivity is constrained by the range of crossover frequencies, $\Delta\omega_0$, exhibited across each subpopulation. Specifically, one wishes to pick internal conductivities that result in EAVs without overlapping dielectrophoretic responses over as large a range of frequencies as possible. For simplicity, we express the internal conductivity as a multiple of the medium conductivity ($\sigma_c = k\sigma_m$ with $k > 1$) To estimate the implications of this requirement, one can approximate the variation in ω_0 associated with variations in both vesicle size and internal conductivity. Equating these variations and assuming $\varepsilon_c \approx \varepsilon_m$ gives:

$$\frac{d\sigma_c}{\sigma_c} = \frac{-\left[2(ac_m)^2(k-1)(k+2) + ac_m\varepsilon_m(k-4)(k+1)\right]}{\left[(ac_m)^2(k-4) + ac_m\varepsilon_m(-3k-8) - 4\varepsilon_m^2(k+1)\right]}\frac{da}{a} \tag{7}$$

By narrowing the size distribution of the EAVs, and choosing the internal conductivity as prescribed approximately by Eq. 7, it is possible to create suspensions comprised of EAVs undergoing dispersions in distinct ranges of frequency. Particularly useful values of k are those for which the crossover frequency is more sensitive to variations in internal conductivity than to variations in size (see Supplemental Figure). For example, a vesicle with $a = 2$ μm, $c_m = 0.002$ F/m^2 and $\varepsilon_m = 80\varepsilon_0$, will be more sensitive to changes in internal conductivity when the internal conductivity is greater than that of the surrounding medium by a factor of ~1.8 or less, with the caveat that if k is too close to unity the crossover frequency will no longer exist (k ~1.45 for these parameters). Alternatively, as described in Eq. 5, operating at high frequency allows one to form multiple electrically distinct vesicles largely independent of the size distribution of the population. Accordingly, even in the presence of considerable polydispersity, it is possible to create populations of particles undergoing transitions from positive to negative polarizability over narrow frequency ranges.

Further control is made possible by modulating the vesicle's membrane capacitance at the same time as its interior conductivity, enabling the creation of EAV populations in which each type of vesicle has a frequency range over which it is the most polarizable member of the population. Increasing the membrane capacitance shifts the spectrum to lower frequencies, whereas increasing the internal conductivity reduces the peak polarizability of the spectra. A population of EAVs for which c_m and σ_c are controlled to vary inversely produces a set of spectra in which each member of the population exhibits the maximum polarizability within the population over a particular range of frequencies.

The modification of giant vesicle membranes with polymers has been the subject of considerable past study[34,35], specifically in the application of studying the effects of polymers on membrane curvature. Additionally, polymers have been encapsulated within the aqueous phase of giant vesicles[36] and have been used to study compartmentalization in aqueous two-phase systems[37]. Thus, polymers such as PEG have served roles in the modification of both the internal aqueous phase properties and external membrane properties[38]. By decorating vesicles with PEG molecules we have further extended the use of polymer functionalizations to affect changes in the electrical properties of vesicles. This ability to modulate the specific

capacitance of membranes has implications from the study of fundamental properties membranes (and the organization of polymers within membranes) and the use of polymer-functionalized vesicles as electrically distinguishable surrogate cells for DEP-based manipulation and separation.

Besides the sign of a particle's polarization in an electric field, a second means of addressing particles is according to the magnitude of their polarization. If we define the dielectrophoretic velocity of a particle as the dielectrophoretic force divided by the Stokes drag coefficient, we have that $U_{DEP} \propto a^2 \, \mathrm{Re}\{\underline{K}(\omega)\}$. The dependence of $\mathrm{Re}\{\underline{K}\}$ on vesicle size at relatively low frequencies can be determined from Eq. 3, with smaller particles typically exhibiting more negative polarizabilities. It is thus possible to minimize the sensitivity of the dielectrophoretic velocity on particle size by choosing a frequency such that $\partial U_{DEP}/\partial a \approx 0$ over the targeted size range. For general sizes and conductivities of interest ($a \sim 1{-}10$ μm and $\sigma_c > \sigma_m$), optimal insensitivity to size is obtained by selecting the frequency according to

$$\omega \cong \frac{2\sigma_m \sigma_c}{(\sigma_c + 2\sigma_m)} \left[\left(1 + \frac{1}{2} \frac{\sigma_c + 2\sigma_m}{\sigma_c - \sigma_m} \right)^{1/2} - 1 \right]^{1/2} \frac{1}{a c_m}$$

(8)

Although this does not remove the dependence of U_{DEP} on size for an arbitrarily large range of sizes, it does improve it significantly. For example, using core and medium conductivities typical for our experiments and operating at a frequency of ~350 kHz, Eq. 8 predicts that vesicles in a size range from $3 - 7$ μm will exhibit dielectrophoretic velocities within 60% of each other, compared to a greater than five-fold difference for particles for which $\mathrm{Re}\{\underline{K}\}$ is independent of particle size.

In all, the ability to generate populations of vesicles with distinct polarizabilities opens new avenues for the study of electric field interactions with phospholipid vesicles. Previous work has focused on using electric fields to apply forces to vesicles to study deformations of phosopholipid membranes[39,40], complex mechanisms of membrane fusion[5], and alterations in vesicle morphology[41]. Thus considerable effort has focused on using electric fields to study vesicles and membranes. Our work opens an avenue of investigation in the use of vesicles to study electric field phenomena, providing the ability to characterize systems that use electric field-based manipulation techniques (such as DEP). Vesicles can now find valuable applications as surrogates for living cells in the characterization of microscale cell manipulation devices.

CONCLUSIONS

We have demonstrated the ability to generate EAVs as test particles for DEP-based microsystems. These vesicles can be specifically engineered to allow for their dielectrophoretic manipulation in microsystems. We have demonstrated the ability to create electrically distinct particles using cross-over frequency measurements with a canonical DEP device. Further, we have shown that it is possible to alter the effective membrane thickness of EAV membranes using PEG-conjugated lipids. This shows that vesicles allow considerable control over their chemical composition (and therefore electrical properties) and lend themselves well to the generation of electrically distinct populations of test particles.

We believe these proof-of-principle studies demonstrate that the electrical properties of vesicles can be specifically engineered to allow their dielectrophoretic manipulation. Moreover, the generation of EAVs form the first steps toward the development of vesicles as metrology tools for DEP-based microsystems.

MATERIALS AND METHODS

EAV Electroformation

EAVs were prepared using a previously described electroformation technique[21]. Briefly, electroformation was performed in a chamber consisting of two 50×75 mm indium tin oxide (ITO) slides (SPI Supplies) separated by a 1-mm-thick silicone gasket (Press-to-seal gaskets, Invitrogen). ITO slides were cleaned in 1% Micro-90 solution, followed by ultrasonicating $2\times$ in acetone and rinsed by ultrasonicating $2\times$ in isopropanol. and subsequently dried with a nitrogen stream. 1-Stearoyl-2-oleoyl-glycero-3-phoshocholine (SOPC, Avanti Polar Lipids) stock solutions at 10 mg/ml concentration were first diluted to 1 mg/ml concentration (in chloroform) and subsequently pipetted on the bottom slide of the electroformation chamber. The lipid solution was then allowed to dry for approximately one hour in a vacuum dessicator. The internal aqueous solution was pipetted in the gasket reservoirs and then capped with the top ITO slide (with the conducting surfaces facing each other) and clamped with binder clips. A sinusoidal waveform (2 Vp-p, 10 Hz) was applied for two hours. For the preparation of fluorescently labeled EAVs, 1 mol% of lissamine rhodamine phosphatidylethanolamine, fluorescein phosphatidylethanolamine, or dansyl phosphatidylethanolamine (respectively, Lissamine rhodamine PE, Fluorescein PE, and Dansyl PE, Avanti Polar Lipids) was added to the 1 mg/ml SOPC solution prior to vacuum drying. For the generation of PEG-conjugated EAVs, 5 mol% of 1,2-distearoyl-glycero-3-phospoethanolamine-N-polyethylene-glycol-2000-carboxyfluorescein (DSPE PEG2 CF, Avanti Polar Lipids) was added to the 1 mg/ml SOPC solution prior to vacuum drying. For the generation of counter-stained PEG-conjugated EAVs, 5 mol% of 1,2-distearoyl-glycero-3-phospoethanolamine-N-polyethylene-glycol-2000-carboxy-fluorescein and 1 mol% of lissamine rhodamine phosphatidylethanolamine was added to 1 mg/ml 1-palmitoyl-2-oleoyl-glycero-3-phoshocholine (POPC, Avanti Polar Lipids).

Light Microscopy

EAVs were imaged immediately after electroformation on an inverted microscope (Axiovert 200, Carl Zeiss Microimaging) using phase microscopy. Once vesicle formation was confirmed, vesicle suspensions were aspirated from the gaskets and re-suspended in iso-osmolar glucose solutions (50 mM). The difference in density allowed for the vesicles to settle to the bottom of the chamber and allowed for ease of imaging on an inverted microscope using both phase and fluorescence microscopy. All phase images were captured at 8 bit resolution using a cooled camera (SPOT RT, Diagnostic Instruments). Fluorescence illumination was provided by an XCite 100 (EXFO Life Sciences and Industrial Division) illumination source. EGFP (Set 38, Carl Zeiss MicroImaging), Texas Red, and DAPI filter sets (31000 and 31002, Chroma Technology) were used for imaging green-fluorescent, red-fluorescent, and blue fluorescent vesicles, respectively. All fluorescence images were captured at 12 bit resolution using a cooled camera (SPOT RT, Diagnostic Instruments).

Image Processing

Fluorescence images of counter-stained PEG-conjugated EAVs were obtained using both red-fluorescent and green-fluorescent filter sets. Red-fluorescent images (representing the lissamine rhodamine labeled lipids) were thresholded and used as a mask for the green-fluorescent images (representing the PEG-lipids). The average fluorescence signal per unit area of membrane was then calculated from the masked green-fluorescence image. A schematic depicting this image processing technique has been included in the Supplemental Information (Figure S1).

Interdigitated Electrode Array Design and Fabrication

Interdigitated electrode (IDE) arrays were fabricated using a standard gold lift-off process on Pyrex substrates that has been previously described[13]. Briefly, 6" Pyrex substrates were cleaned in a piranha solution and subsequently rinsed. Image reversal resist (AZ5214, Clariant) was spun on the wafers and the wafers were pre-baked at 90 °C for 30 minutes. Subsequently, wafers were exposed at 10 mJ/cm^2 through a custom-designed chrome photolithography mask (Fineline Imaging) for 5 seconds and then post-baked for 30 minutes at 120 °C. Wafers were then flood exposed for 10 seconds and developed for ~1 minute. A 100 Å of titanium and 1000 Å of gold were then deposited using an electron-beam deposition system. The resist was subsequently removed by immersion in an acetone bath overnight. The wafers were then diced with a diamond saw to yield individual chips.

Interdigitated Electrode Array Packaging

For our IDE devices, we packaged individual chips by mounting them on glass slides using double-sided tape. We then affixed the slides to a standard upright microscopy stage insert. We used laser-cut PDMS gaskets (250 μm thick, Bisco Silicones Inc.) around the active chip areas to form flow chambers. We then filled the chambers with vesicle suspensions and capped them with coverslips. We made electrical connections to the on-chip electrodes using alligator clips and delivered signals using an arbitrary waveform generator (Agilent 33250A).

Cross-over frequency measurements

We measure the crossover frequencies of vesicles and fluorescent polystyrene beads (F8834, Invitrogen) using an interdigitated electrode array in which the pitch and spacing of the electrodes are both 50 μm. By diluting EAV solution (with some volume fraction of EAVs) with deionized water at a ratio of 2:1, we set the conductivity of the external medium to approximately half that of the vesicle interior. We pipette ~10μl of the diluted EAV suspension into a laser-cut silicone gasket placed over the electrode array and seal the chamber with a glass coverslip. The device is placed under a fluorescence microscope (Zeiss AxioImager, Carl Zeiss MicroImaging) and imaged using a 20× (0.5 NA) objective. Individual EAVs are selected so as to broadly sample the total distribution of sizes, down to approximately 1 μm. The electrodes are then activated at 3−5 Vp-p and frequencies ranging from ~50kHz – 1MHz while we observe the behavior of the vesicle. We narrow the range of excitation frequencies until the vesicle exhibits minimal response to the application of the electric field. We supplement this determination of the crossover frequency with an image of the vesicle, from which we determine its radius.

Supplementary Material

Refer to Web version on PubMed Central for supplementary material.

ACKNOWLEDGEMENTS

REFERENCES

1. Long MS, Jones C, Helfrich MR, Mangeney-Slavin LK, Keating CD. Dynamic microcompartmentation within synthetic cells. Proc. Natl. Acad. Sci 2005;102:5920–5925. [PubMed: 15788532]

2. Long MS, Cans A-S, Keating CD. Budding and asymmetric protein microcompartmentation in giant vesicles containing two aqueous phases. J. Am. Chem. Soc 2008;130:756–762. [PubMed: 18092782]

3. Upadhyaya A, Chabot JR, Andreeva A, Samadani A, van Oudenaarden A. Probing polymerization forces by using actin-propelled lipid vesicles. Proc. Natl. Acad. Sci 2003;100:4521–4525. [PubMed: 12657740]

4. Noireaux V, Libchaber A. A vesicle bioreactor as a step toward an artificial cell assembly. Proc. Natl. Acad. Sci 2004;101:17669–17674. [PubMed: 15591347]

5. Haluska CK, Riske KA, Marchi-Artzner V, Lehn J-M, Lipowsky R, Dimova R. Timescales of membrane fusion revealed by direct imaging of vesicle fusion with high temporal resolution. Proc. Natl. Acad. Sci 2006;103:15841–15846. [PubMed: 17043227]

6. Tan Y-C, Hettiarachchi K, Siu M, Pan Y-R, Lee AP. Controlled Microfluidic Encapsulation of Cells, Proteins and Microbeads in Lipid Vesicles. J. Am. Chem. Soc 2006;128:5656–5658. [PubMed: 16637631]

7. Yoshikawa K, Nomura S-I. Giant phospholipid vesicles entrapping giant DNA. Giant Vesicles. Perspectives in Supramolecular Assemblies 2000;6:313–317.

8. Ratanabanangkoon P, Gropper P, Merkel M, Sackmann E, Gast AP. Mechanics of streptavidin-coated giant lipid bilayer vesicles: A micropipet study. Langmuir 2003;19:1054–1062.

9. Ratanabanangkoon P, Gropper P, Merkel M, Sackmann E, Gast AP. Two-dimensional streptavidin crystals on giant lipid bilayer vesicles. Langmuir 2002;18:4270–4276.

10. Albrecht DR, Underhill GH, Mendelson A, Bhatia SN. Multiphase electropatterning of cells and biomaterials. Lab Chip 2007;7:702–709. [PubMed: 17538711]

11. Ho C-T, Lin R-Z, Chang W-Y, Chang H-W, Liu C-H. Rapid heterogenous liver-cell on-chip patterning via the enhanced field-induced dielectrophoresis trap. Lab Chip 2006;6:724–734. [PubMed: 16738722]

12. Gray DS, Tan JL, Voldman J, Chen CS. Dielectrophoretic registration of living cells to a microelectrode array. Biosensors and Bioelectronics 2004;19:1765–1774. [PubMed: 15198083]

13. Gadish N, Voldman J. High-Throughput Positive-Dielectrophoretic Bioparticle Microconcentrator. Anal. Chem 2006;78(22):7870–7876. [PubMed: 17105182]

14. Yang L, Banada PP, Chatni MR, Lim KS, Bhunia AK, Ladisch M, Bashir R. A multifunctional micro-fluidic system for dielectrophoretic concentration coupled with immuno-capture of low numbers of *Listeria monocytogenes*. Lab Chip 2006;6:896–905. [PubMed: 16804594]

15. Lapizco-Encinas BH, Simmons BA, Cummings EB, Fintschenko Y. Dielectrophoretic concentration and separation of live and dead bacteria in an array of insulators. Anal. Chem 2004;76:1571–1579. [PubMed: 15018553]

16. Taff BM, Voldman J. A Scalable Addressable Positive-Dielectrophoretic Cell-Sorting Array. Anal. Chem 2005;77:7976–7983. [PubMed: 16351145]

17. Hawkins BG, Smith AE, Syed YA, Kirby BJ. Continuous-Flow Particle Separation by 3D Insulative Dielectrophoresis Using Coherently Shaped, dc-Biased, ac Electric Fields. Anal. Chem 2007;79(19):7291–7300. [PubMed: 17764153]

18. Braschler T, Demierre N, Nascimento E, Silva T, Oliva AG, Renaud P. Continuous separation of cells by balanced dielectrophoretic forces at multiple frequencies. Lab Chip 2008;8:280–286. [PubMed: 18231667]

19. Vykoukal J, Vykoukal DM, Sharma S, Becker FF, Gascoyne PRC. Dielectrically Addressable Microspheres Engineered Using Self-Assembled Monolayers. Langmuir 2003;19:2425–2433.

20. Chan K–L, Gascoyne PRC, Becker FF, Pethig R. Electrorotation of liposomes: verification of dielectric multi-shell model for cells. Biochim. Biophys. Acta 1997;1349(2):182–96. [PubMed: 9421190]

21. Angelova MI, Dimitrov DS. Liposome Electroformation. Faraday Discuss. Chem. Soc 1986;81:303–312.

22. Jones, TB. Electromechanics of Particles. Cambridge Univ. Press; Cambridge: 1995.

23. Gascoyne PRC, Wang X-B, Huang Y, Becker FF. Dielectrophoretic separation of cancer cells from blood. IEEE Transactions on Industry Applications 1997;33(3):670–678.

24. Marsh D, Bartucci R, Sportelli L. Lipid membranes with grafted polymers: physicochemical aspects. Biochim. Biophys. Acta 2003;1615:33–59. [PubMed: 12948586]

25. Milner ST, Witten TA, Cates ME. A parabolic density profile for grafted polymers. Europhys. Lett 1988;5:413–418.

26. Evans E, Klingenberg DJ, Rawicz W, Szoka F. Interactions between polymer-grafted membranes in concentrated solutions of free polymer. Langmuir 1996;12:3031–3037.

27. Marsh, D. Handbook of Lipid Bilayers. CRC Press; Boca Raton, FL: 1990.

28. Kenworthy AK, Hristova K, Needham D, McIntosh TJ. Range and magnitude of the steric pressure between bilayers containing phospholipids with covalently attached poly(ethylene glycol). Biophys. J 1995;68:1921–1936. [PubMed: 7612834]

29. Kuhl TL, Leckband DE, Lasic DD, Israelachvili JN. Modulation of interaction forces between bilayers exposing short-chained ethylene oxide headgroups. Biophys. J 1994;66:1479–1488. [PubMed: 8061197]

30. Hermanson KD, Lumsdon SO, Williams JP, Kaler EW, Velev OD. Dielectrophoretic assembly of electrically functional microwires from nanoparticle suspensions. Science 2001;294:1082–1086. [PubMed: 11691987]

31. Taylor P, Xu C, Fletcher PDI, Paunov VN. Fabrication of 2D arrays of giant liposomes on solid substrates by microcontact printing. Phys. Chem. Chem. Phys 2003;5:4918–4922.

32. Funakoshi K, Suzuki H, Takeuchi S. Formation of giant lipid vesicle-like compartments from a planar lipid membrane by a pulsed jet flow. J. Am.Chem. Soc 2007;129:12608–12609. [PubMed: 17915869]

33. Needham, D. Permeability and Stability of Lipid Bilayers. Disalvo, EA.; Simon, SA., editors. CRC Press; Boca Raton, FL: 1995. p. 49-73.

34. Nikolov V, Lipowsky R, Dimova R. Behavior of Giant Vesicles with Anchored DNA Molecules. Biophys. J 2007;92:4356–4368. [PubMed: 17384074]

35. Sapper A, Janshoff A. Electrically Induced Deformation of Giant Liposomes Monitored by Thickness Shear Mode Resonators. Langmuir 2006;22:10869–10873. [PubMed: 17154553]

36. Dominak LM, Keating CD. Polymer Encapsulation within Giant Lipid Vesicles. Langmuir 2007;23:7148–7154. [PubMed: 17516666]

37. Helfrich MR, Mangeney-Slavin LK, Long MS, Djoko KY, Keating CD. Aqueous Phase Separation in Giant Vesicles. J. Am. Chem. Soc 2002;124:13374–13375. [PubMed: 12418876]

38. Needham D, Kim DH. PEG-covered lipid surfaces: bilayers and monolayers. Colloids Surf. B 2000;18:183–195.

39. Korlach J, Reichle C, Muller T, Schnelle T, Webb WW. Trapping, deformation, and rotation of giant unilamellar vesicles in octode dielectrophoretic field cages. Biophys. J 2005;89:554–562. [PubMed: 15863477]

40. Riske KA, Dimova R. Electrical pulses induce cylindrical deformations on giant vesicles in salt solutions. Biophys. J 2006;91:1778–1786. [PubMed: 16766621]

41. Aranda S, Riske KA, Lipowsky R, Dimova R. Morphological transitions of vesicles induced by AC electric fields. Biophys. J 2008;95:L19–L21. [PubMed: 18487308]
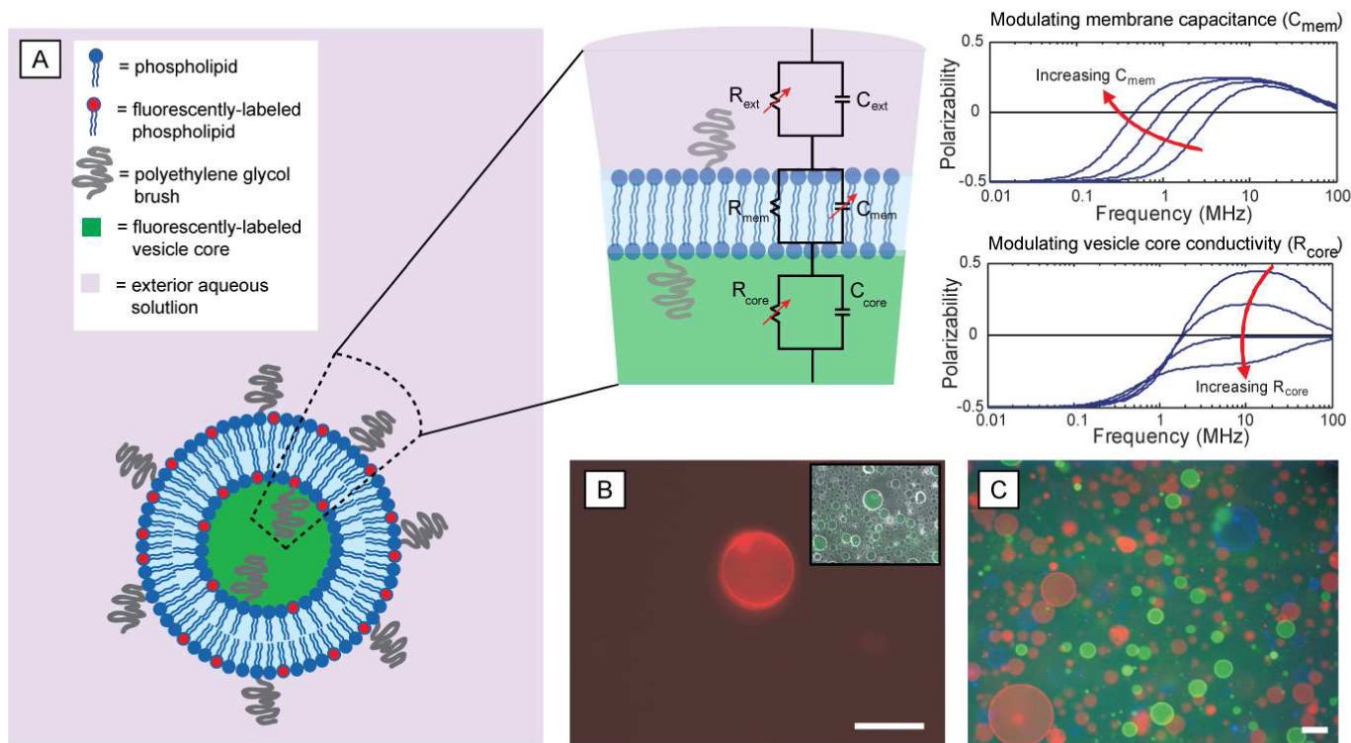
Figure 1. Electrically addressable vesicles (EAVs)
(A) Schematic (not to scale) of an EAV where we have independent control over the properties of the vesicle membrane and aqueous core. Control of vesicle membrane and aqueous membrane properties result in distinct electrical polarizabilities and consequently identifiable dielectrophoretic responses. Modulating the membrane capacitance with PEG brushes (schematic, center panel) results in shifting of the DEP spectra towards lower frequencies (plot, upper panel). Modulating the aqueous core conductivity by altering the ionic strength of the encapsulated solution results in lowering the peak polarizability of the respective DEP spectra (plot, low panel). (B) Demonstration of control of membrane and aqueous core properties. Fluorescence microscopy image of a representative EAV with lissamine-rhodamine-labeled membrane. The inset shows merged phase and fluorescence microscopy images with encapsulation of fluorescein salt (green) in the aqueous core of EAVs. (C) Merged fluorescence image of a population of differentially labeled EAVs - lissamine-rhodamine (red, lipid), carboxyfluorescein (green, aqueous core) and dansyl PE (blue, lipid). Scale bars 50 μm.
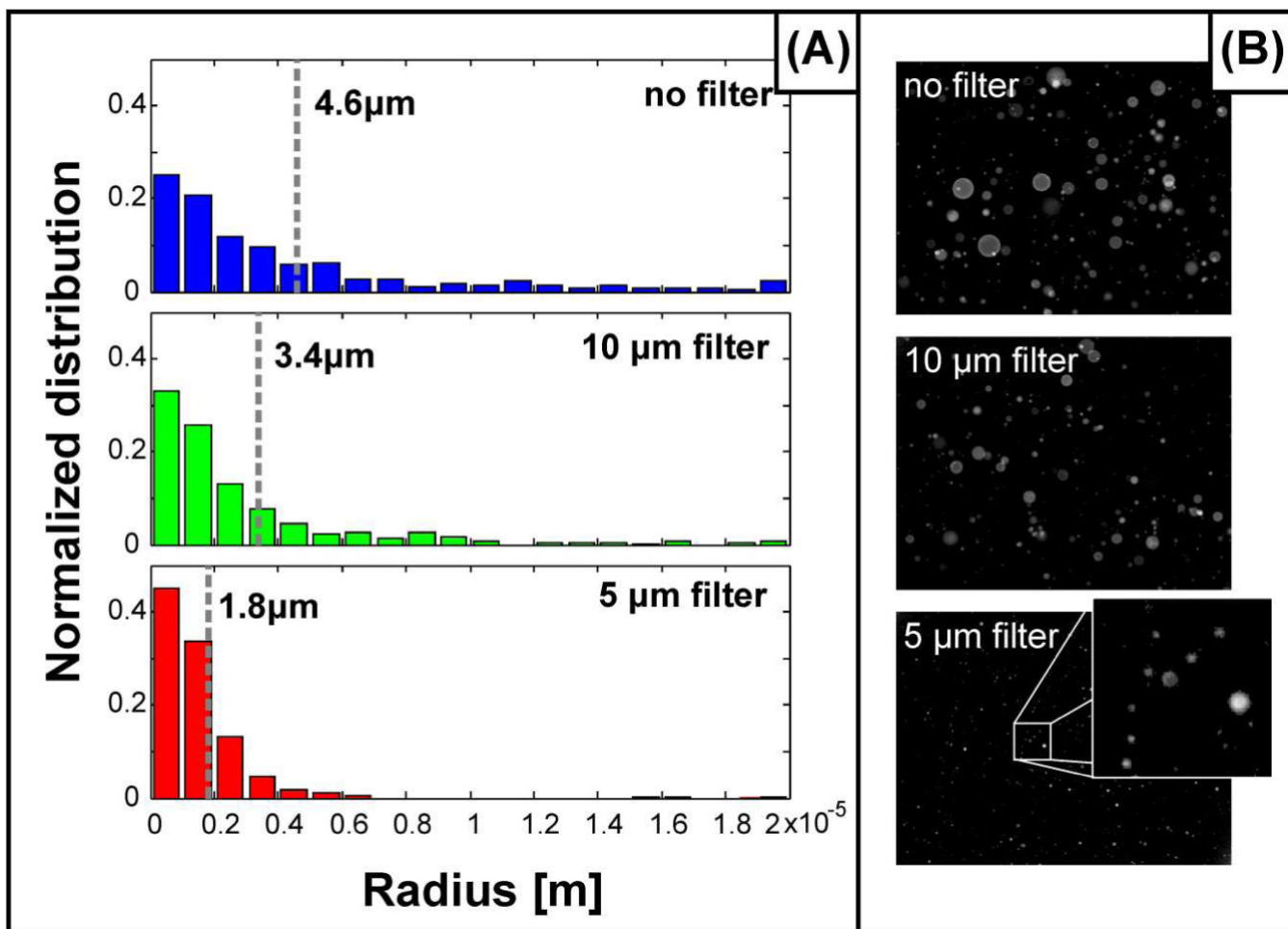
Figure 2. Biasing EAV size
(A) Histograms with 1 μm bins of size distribution of EAVs after filtration through different size pores (red bars: 5 μm, green bars: 10 μm, and blue bars: unfiltered). Dashed lines and accompanying numbers indicate the mean vesicle size for each of the three cases − 1.8 μm for a 5 μm filter, 3.4 μm for a 10 μm filter and 4.6 μm for unfiltered. (B) Fluorescence microscopy images before (top) and after filtering through 5 μm (middle) and 10 μm (bottom) filters showing that EAVs can be selected based on size.
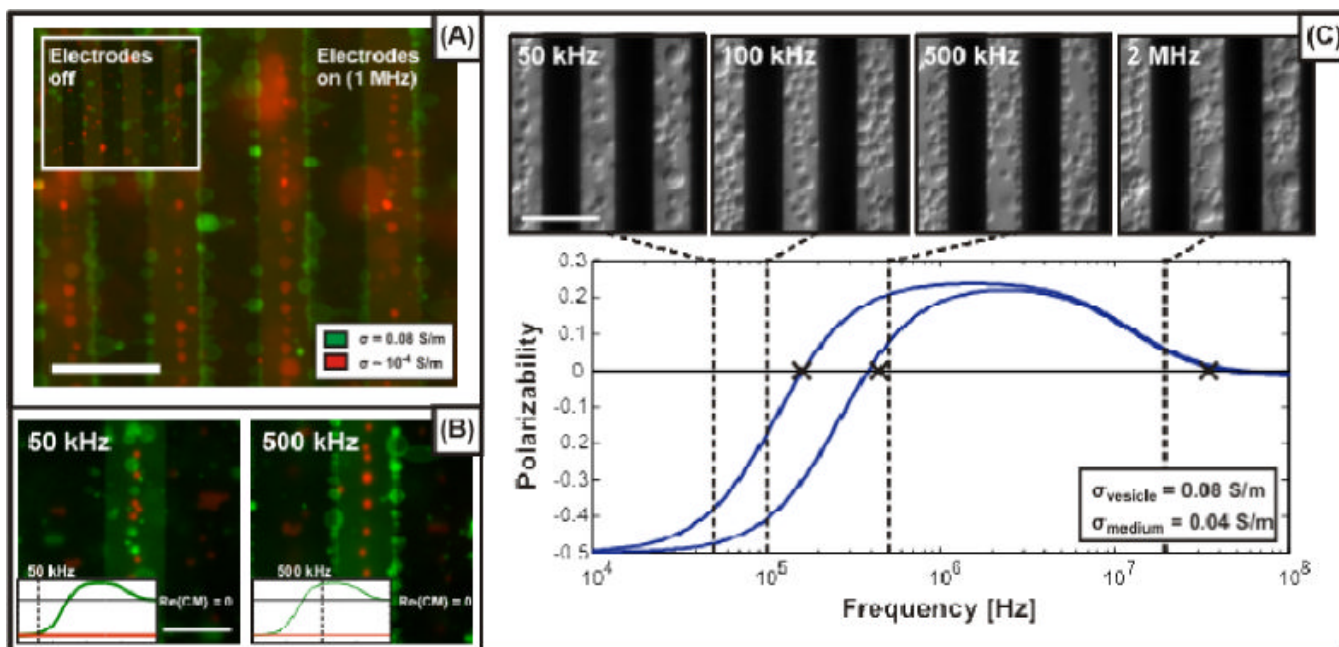
Figure 3. Controlling the dielectric spectra of EAVs
(A) Fluorescence microscopy images of EAVs suspended in a medium with a conductivity of 0.04 S/m above an interdigitated electrode array before (inset) and after applying a 1 MHz electric field, showing the different DEP responses of the red ($\sigma_c \sim 10^{-4}$ S/m) and green ($\sigma_c = 0.08$ S/m) EAVs. Scale bar 50 μm. (B) Comparison of the dielectrophoretic response of EAVs (green, $\sigma_c = 0.08$ S/m) and polystyrene beads (red) in a medium with conductivity 0.04 S/m. While the beads exhibit a uniform n-DEP response across several orders of magnitude in frequency, the EAVs transition from negative to positive polarizability. Scale bar 25 μm. Insets show plots of the real value of the CM-factor across frequency (with the dashed lines indicating frequencies at which the electrodes were stimulated during image capture). (C) The DEP spectra of EAVs with an interior conductivity twice that of the surrounding medium. Curves for EAVs with radii of 5 and 12 μm are obtained by fitting crossover frequency measurements to the single shell model of Eq. 2. EAVs of different sizes exhibit different membrane capacitances, resulting in the differences in spectra seen between ~10kHz and 1 MHz. The micrographs above the curves highlight the behavior of an EAV suspension at the indicated frequencies. As the frequency is increased, the EAVs' polarizabilities range from strongly negative (at 50 kHz, indicated in the figure by the exclusion of EAVs from the electrode edges), to weakly negative (100 kHz), to strongly positive (500 kHz, indicated by the accumulation of EAVs at the electrode edge), to nearly zero (at 2 MHz). Scale bar 50 μm.
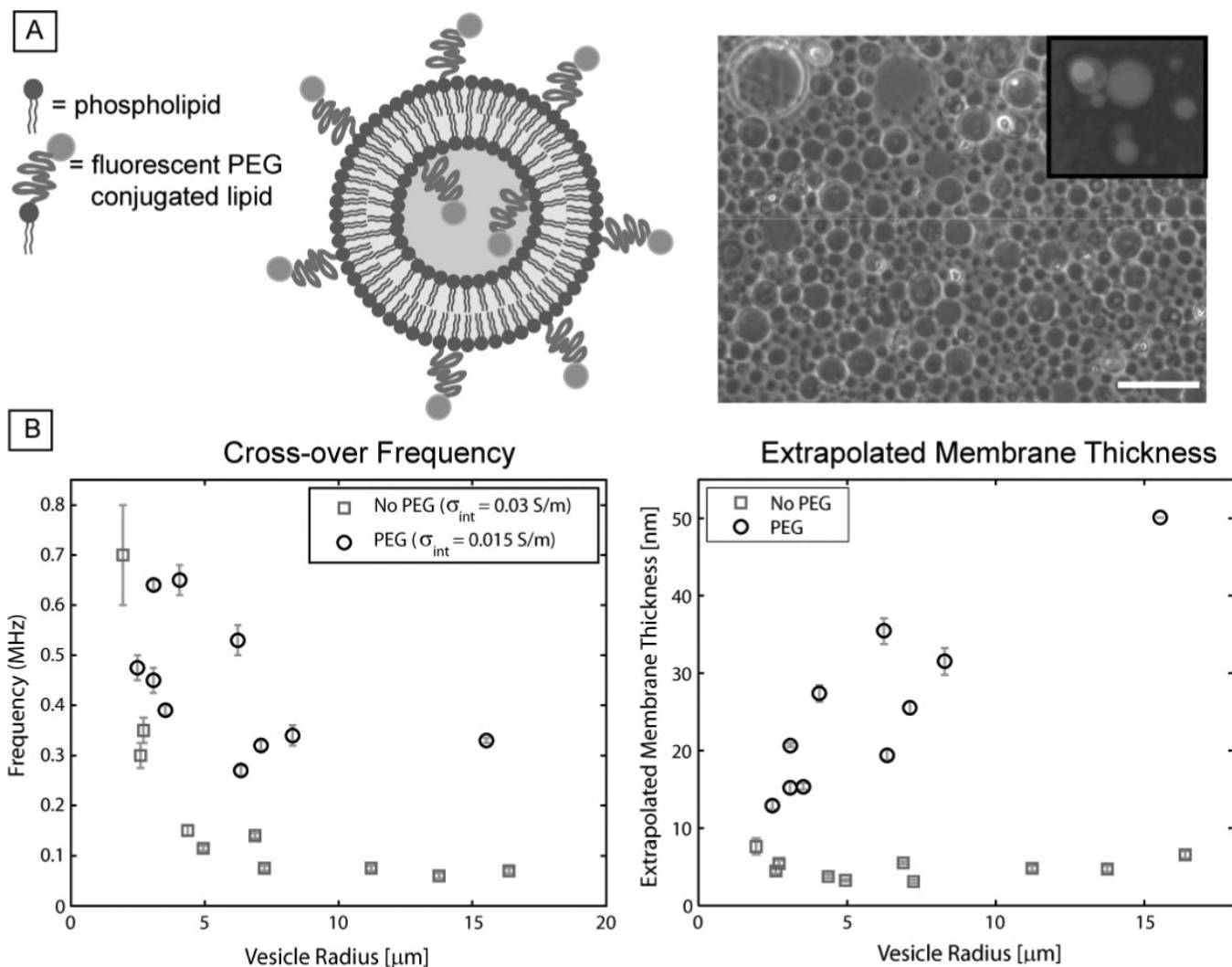
Figure 4. Modulating membrane thickness
(A) Schematic of PEG-modified EAV (not drawn to scale) along with phase microscopy images of electroformed EAVs (the inset shows fluorescence images of the EAVs, confirming that they are PEG-modified). Scale bar 50 μm. (B) Plot of EAV radius versus cross-over frequency and plot of estimated effective membrane thickness. While EAVs formed in the absence of PEG show a uniform membrane thickness of ~5 nm, as expected for a single lipid bilayer, PEG-modified EAVs exhibit an increased effective membrane thickness that varies with radius. This suggests that the presence of PEG does more than change the thickness of the membrane, perhaps significantly altering the EAV's surface conductance and/or permittivity as well. For both PEGylated and non-PEGylated vesicles, the medium conductivity used for these measurements was half that of the vesicle interior.